BMC Structural Biology

Research article

Low-resolution structural studies of human Stanniocalcin-1

Daniel M Trindade[1,2], Júlio C Silva[3,4], Margareth S Navarro[1], Iris CL Torriani[3,4] and Jörg Kobarg*[1,2]

Address: [1]Centro de Biologia Molecular Estrutural (CEBIME), Campinas, SP, Brazil, [2]Instituto de Biologia, Departamento de Bioquímica, Universidade Estadual de Campinas, Campinas, SP, Brazil, [3]Instituto de Física "Gleb Wataghin", Universidade Estadual de Campinas, Campinas, SP, Brazil and [4]Laboratório Nacional de Luz Síncrotron (LNLS), Campinas, SP, Brazil

Email: Daniel M Trindade - danielmt@lnls.br; Júlio C Silva - jsilva@lnls.br; Margareth S Navarro - msugano@lnls.br; Iris CL Torriani - torriani@lnls.br; Jörg Kobarg* - jkobarg@lnls.br

* Corresponding author

Published: 27 August 2009

BMC Structural Biology 2009, **9**:57 doi:10.1186/1472-6807-9-57

Received: 17 March 2009
Accepted: 27 August 2009

This article is available from: http://www.biomedcentral.com/1472-6807/9/57

Abstract

Background: Stanniocalcins (STCs) represent small glycoprotein hormones, found in all vertebrates, which have been functionally implicated in Calcium homeostasis. However, recent data from mammalian systems indicated that they may be also involved in embryogenesis, tumorigenesis and in the context of the latter especially in angiogenesis. Human STC1 is a 247 amino acids protein with a predicted molecular mass of 27 kDa, but preliminary data suggested its di- or multimerization. The latter in conjunction with alternative splicing and/or post-translational modification gives rise to forms described as STC_{50} and "big STC", which molecular weights range from 56 to 135 kDa.

Results: In this study we performed a biochemical and structural analysis of STC1 with the aim of obtaining low resolution structural information about the human STC1, since structural information in this protein family is scarce. We expressed STC1 in both *E. coli* and insect cells using the baculo virus system with a C-terminal 6 × His fusion tag. From the latter we obtained reasonable amounts of soluble protein. Circular dichroism analysis showed STC1 as a well structured protein with 52% of alpha-helical content. Mass spectroscopy analysis of the recombinant protein allowed to assign the five intramolecular disulfide bridges as well as the dimerization Cys202, thereby confirming the conservation of the disulfide pattern previously described for fish STC1. SAXS data also clearly demonstrated that STC1 adopts a dimeric, slightly elongated structure in solution.

Conclusion: Our data reveal the first low resolution, structural information for human STC1. Theoretical predictions and circular dichroism spectroscopy both suggested that STC1 has a high content of alpha-helices and SAXS experiments revealed that STC1 is a dimer of slightly elongated shape in solution. The dimerization was confirmed by mass spectrometry as was the highly conserved disulfide pattern, which is identical to that found in fish STC1.

Background

Stanniocalcins (STCs) represent a small family of secreted glycoprotein hormones consisting of STC1 and STC2 in which amino acid sequences are highly conserved among aquatic and terrestrial vertebrates [1-7]. However, the lack of homology with other known proteins has hampered the understanding of their functions. Initial evidence suggested that mammalian STC1 would parallel the function of fish STC1, which has been implicated in mineral homeostasis [8-10]. It is tempting to assume that the functions of STC1 and STC2 overlap at least in part, since they share high similarity in their primary amino acid sequence especially at the N-terminus and the pattern of cysteine residues is highly conserved [11].

However, there are also several differences between STC1 and STC2, including the fact that STC2 has 55 additional amino acids, the majority of which are located at its C-terminus [12-14]. Furthermore their expression patterns are different[1,14-17] and STC2 is unable to displace STC1 from its putative receptor [18,19], indicating that both molecules may have distinct receptors.

Although STC1 functions as an anti-hypercalcemic hormone in fish [20-22], it is becoming increasingly clearer that it may have expanded roles in mammals. Such assumption is based on its wide expression pattern in adult normal tissues[1,16,23-27], tumors [17,28,29] and also during embryogenesis [30-35]. Further support for a complex function of STC1 in mammals comes from studies that show its varying sub-cellular localizations [18,19] and of a gain-of-function phenotype observed in transgenic mouse [36,37].

Relatively little is also known about STCs molecular structure. The human and mouse genomes encode a 247 amino acid STC1 protein [17,38]. The first 204 amino acids show 92% sequence similarity to salmon STC1 and include a conserved N-linked glycosylation site of the type Asn-X-Thr/Ser (N-X-T/S) [17,39]. Compared to the fish STC1 however, the last 43 residues at the C-terminus are poorly conserved in human STC1 (and STC2), suggesting that the main biological activity of the STCs is mediated through its N-terminus [40,41].

In ancient fish, the last conserved cysteine residue in the C-terminal of STC1, which is supposedly involved in its dimerization, is replaced by arginine or histidine residues, thereby giving rise to a strictly monomeric form of the protein [42,43]. Although dimeric forms of STC1 have been described [39,44,45], answers to the question of its potential multimerization and modification to diverse higher molecular weight forms under certain circumstances remain elusive.

STC1 however, seems to exist in two different forms, the conventional dimeric 56 kDa form, consisting of two ~28 kDa monomers, also known as STC_{50}, and a number of higher molecular weight STC variants, collectively referred to as "big STC" [19,25,46-49]. At least three molecular weights: 84, 112, and 135 kDa have been described and big STC1 has been reported to be expressed in adipocytes, adrenocortical cells [47,48] and ovaries [19,25,49]. In order to explain the increased mass of big STC1 it has been suggested that either distinct post-translational modifications, including glycosylation [17,25] or phosphorylation [50] occur in big STC or additional but yet uncharacterized exons [48] are being employed. In agreement with the latter, the monomeric form big STC1 is about ~10 kDa larger than the theoretically predicted monomer. Another possibility is the formation of tri- (84 kDa), tetra- (112 kDa) or even pentamers (140 kDa) of STC1, although in this case obtained values only add up for the theoretically predicted monomer (~28 kDa) but not for that observed for the big STC monomer (~38 kDa). It is however noteworthy that the 135-kDa variant of big STC1 found in adrenocortical cells is resistant to chemical reduction, just like STC_{50} from the mitochondrial matrix [48], thereby suggesting the formation of a more stable and maybe durable quaternary structure.

In this paper we present structural information about the human STC1 protein. We expressed human STC1 in insect cells using a bi-cistronic baculovirus construct. After affinity purification we collected SAXS data for STC1 in solution. Data analyses are indicative of a dimeric protein in solution. Furthermore, we were able to confirm the formation of the conserved disulfide bridges, previously reported in fish STC1, by mass spectrometry.

Results and Discussion

STC1 is predicted to be dimer and to possess a high content of alpha-helices

By analysing the human STC1 amino acid sequence using six different secondary structure prediction databases, we created a secondary structure consensus and scored it by the number of times (one to six times) the predicted secondary structure element scored positive (Figure 1). Prediction programs used were: **PredictProtein/PROF** [51], **PsiPRED** [52], **Predator** [53], **SOPMA** [54], **SSPro** [55] and **JCFO** [56].

In summary, the secondary structure analysis suggested that about 34% of the amino acid sequence of STC1 may form alpha-helices.

We further performed some predictions about ordered or disordered regions within the sequence using **FoldIndex** [57] and **DisEMBL** [58]) as well as **GlobPlot** [59] as a pre-

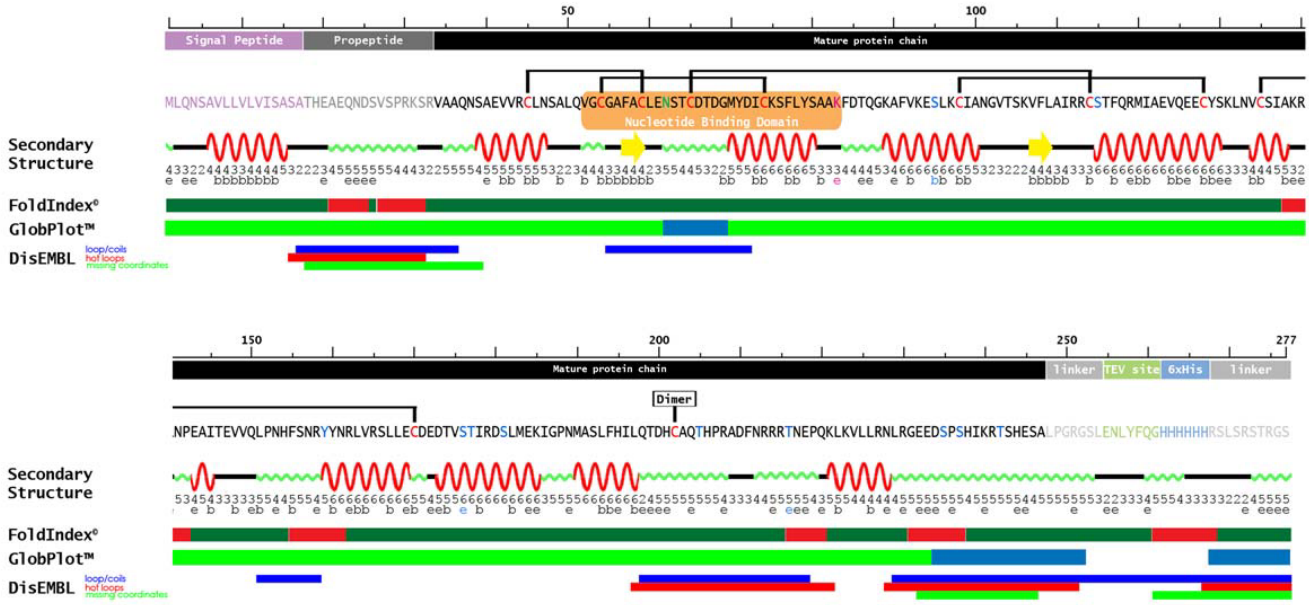

Figure 1

Prediction of secondary structure and putative post-translational modification sites in the human STC1 amino acid sequence. Linear representation of STC1-HT amino acid sequence with assignment of its different regions from N- to C-terminus: signal peptide (purple), pro-peptide (dark gray), mature protein (black), linker regions (light grey), TEV protease cleavage site (green) and 6 × His-tag (light blue). In the amino acid sequence, relevant residues are emphasized by the following color code: Cys: red, Asp predicted to be N-glycosylated: green, Lys predicted to be sumoylated: magenta, Ser, Thr e Tyr residues predicted to be phosphorylated: blue. The conserved pattern of experimentally determined disulfide bridges from salmon STC1 is indicated by black horizontal brackets. Similarly the homo-dimerization Cys is indicated in black (dimer). Below the sequence there is a schematic representation of the predicted consensus secondary structure, obtained by six different prediction programs (red: alpha helix, yellow: beta-sheet, green: coil regions, black: not assigned). The numbers below the secondary structure represent the score (16, indicating how many of the six programs predicted the respective secondary structure element). Furthermore, in a second line, a prediction indicates whether a residue is exposed (e) or buried (b). At the bottom, predictions of three programs for ordered/disordered regions are given: FoldIndex (red: unfolded, green: folded), GlobPlot (green: globular, blue: disordered) and DisEMBL (blue: loops or coils, red: hot loops, green: missing coordinates).

dictor for more globular regions (Figure 1). The first two programs both predicted that the pro-peptide region and possibly the C-terminal region, this last one which contains the Cys disulfide mediated dimerization region, to be highly disorder or a region with high loop/turn content.

We analyzed and plotted (Figure 1) the conserved cysteine residues as well as the experimentally determined disulfide bridges from the salmon sequence determination [39], the signal peptide, pro-peptide and mature protein sequence as annotated at UniProtKB/Swiss-Prot database (Swiss-Prot:P52823), and we also emphasize a previously described nucleotide binding domain (NBD) [60].

Additionally, some predictions about post-translational modifications were performed and compared to published experimental data. An N-glycosylation site which had already been characterized for STC1 [17,41,61] was also predicted by **NetGlyc** [62] (Figure 1)

For phosphorylation analysis we combined prediction data from **NetPhos** [63] and **NetPhosK** [64] together with *in vitro* phosphorylation data [50] to annotate tyrosine, threonine and serine residues as putative phosphorylation sites (Table 1). Most of the kinases that were found to phosphorylate STC1 by the in vitro phophorylation screening of Jellinek and coworkers were predicted by both prediction programs (Table 1), except calmodulin-dependent protein kinase (CaMPK-II) and casein kinase II (CK2).

Analysis by **PredictProtein/PHD Acc** [51] revealed that some of the residues such as S_{176} and T_{216}, are predicted to be exposed to the solvent and therefore more likely to suf-

Table 1: Prediction of putative post-translational modification sites in human STC1.

Residue	Modification	Buried/Exposed Residue[51]	Predictor (Score)	Ref.
N_{62}	N-glycosylation	nd	NetGlyc (0.61)	[17,39,41,61]
K_{83}	Sumoylation	e	SUMOplot™ (0.79)	$
S_{95}	PKC* phosphorylation	b	NetPhos (0.844)/NetPhosK (0.630)	[50]
S_{115}	PKC* phosphorylation PKA* phosphorylation RSK* phosphorylation	nd nd nd	NetPhos (0.788)/NetPhosK (0.722) NetPhos (0.788)/NetPhosK (0.841) NetPhos (0.788)/NetPhosK (0.601)	[50] [50] nd
Y_{159}	INSR* phosphorylation	nd	NetPhos (0.929)/NetPhosK (0.539)	nd
S_{176}	PKC* phosphorylation	e	NetPhos (0.938)/NetPhosK (0.630)	[50]
T_{177}	PKC* phosphorylation	nd	NetPhos (0.983)/NetPhosK (0.640)	[50]
S_{181}	PKA* phosphorylation	nd	NetPhos (0.993)/NetPhosK (0.647)	[50]
T_{205}	PKC* phosphorylation Cdc2* phosphorylation	nd nd	NetPhos (0.606)/NetPhosK (0.815) NetPhos (0.606)/NetPhosK (0.509)	[50] [50]
T_{216}	PKG* phosphorylation	e	NetPhos (0.817)/NetPhosK (0.600)	[50]
S_{235}	GSK3* phosphorylation Cdk5* phosphorylation	nd nd	NetPhos (0.986)/NetPhosK (0.508) NetPhos (0.986)/NetPhosK (0.551)	[50] [50]
S_{237}	PKC* phosphorylation	nd	NetPhos (0.531)/NetPhosK (0.647)	[50]
T_{242}	PKG* phosphorylation	nd	NetPhos (0.523)/NetPhosK (0.693)	[50]

High score predictions of glycosylation, sumoylation and phosphorylation on STC1 sequence are presented. Predicted modifications within the propeptide region were excluded. Putative phosphorylated residues shown here are only those that were both predicted with the highest scores by the NetPhos server and additionally were predicted by NetPhosK, which suggests a specific kinase for the same site. References are related to additional experimental support for the predicted modification, if available. * indicate kinase as predicted by NetPhosK [protein kinase A C or G (PKA; PKC and PKG); 90-kDa Ribosomal S6 Kinase (pp90RSK or RSK); Insulin receptor (INSR); cell division cycle 2 (cdc2 or p34 protein kinase); ciclin dependent kinase 5 (cdk5); Glycogen synthase kinase 3 (GSK3)]; e = exposed residue, b = buried residue, nd = not determined; $ = unpublished data.

fer phosphorylation. Indeed, both residues refer to STC1 kinase sites found to be phosphorylated by Jellinek and co-workers [50].

In order to screen for lysine residues predicted which may be sumoylated in STC1 we used SUMOplot™ http://www.abgent.com/tools/sumoplot and found three putative sumoylated residues (data not shown). The one having the highest score is located at the end of the NBD and the sumoylated residue (K_{83}) is also predicted by **PredictProtein/PHD Acc** to be exposed to solvent. Most interestingly, we found that STC1 interacted with the SUMO1 protein in a yeast two hybrid screen (unpublished data). These data suggest that further experiments should be performed to test if sumoylation of STC1 may occur in vivo, in human cells.

Optimization of the expression and purification of STC1

Our first attempt to produce STC1 in *E. coli* using the HT-STC1ΔNterm construct (Figure 2A) resulted in completely insoluble expression (Figure 2B). Even splitting the protein in two halves using His-tag fusion did not make any difference in solubility, since both parts still expressed in insoluble form (data not shown). Only together with the use of GST-tag (GST-C STC1) we could obtain some soluble expression, however at very low amounts. The highest rate of soluble expression could be obtained with GST-C STC1 (Figure 2C and 2D).

On the other hand, using a modified bi-cistronic vector of the baculovirus expression system we could obtain milligrams per liter of the soluble full-length his-tagged STC1 (STC1-HT) secreted into the media (Trindade et al.,

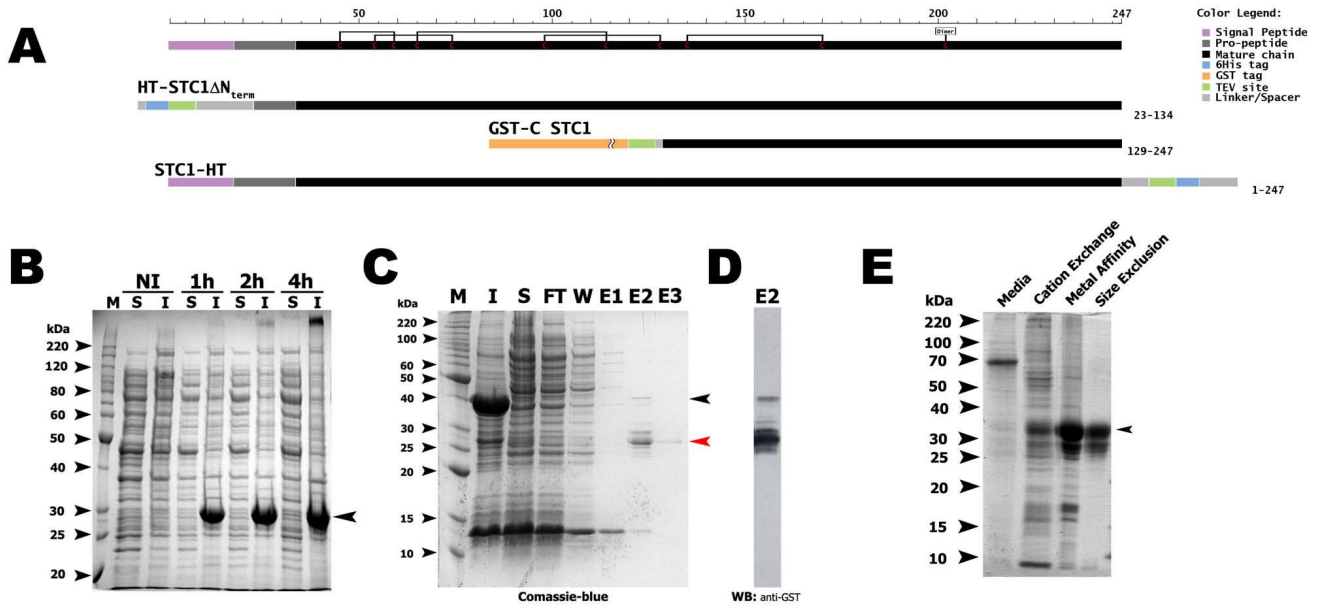

Figure 2

Large scale STC1 expression in E. coli and in insect cells and its purification. **(A)** Tested STC constructs (from top to bottom): an amino-6 × His tagged STC1 without the N-terminal portion which includes the signal peptide (HT-STC1ΔNterm), an amino-GST tagged C-terminal fragment of STC1 (GST-C STC1) and a full length carboxy-6 × His tagged STC1 (STC1-HT). At the right side of each construct is shown the amino acid residues from native STC1 present on that construct. **(B)** Expression test of HT-STC1ΔNterm. Coomassie-blue stained SDS-PAGE of soluble (S) and insoluble (I) fractions expressed in BL21DE3 non-induced (NI) or induced for indicated periods with 0.5 mM IPTG in LB at 37°C. **(C)** GST-C STC1 purification by affinity chromatography using glutathione sepharose beads. Coomassie-blue stained SDS-PAGE of insoluble (I), soluble (S), flow-through (FT), wash (W) and elution (E1-E3) fractions. **(D)** Western blot anti-GST of E2 fraction of purification shown in C. Black arrow heads at right indicate expected recombinant protein size and red arrow head indicates un-fused GST protein. **(E)** Expression and purification of STC1-HT from insect cells (using the baculo virus system): Coomassi-blue stained SDS-PAGE of peak-fractions after cation exchange, metal affinity and Size Exclusion chromatography. Arrow head indicates expected size of recombinant expressed protein. Invitrogen Bench Marker protein ladder (M).

unpublished data). The amount of virus and of infected cells could be easily optimized, since the recombinant bicistronic baculo virus promotes production of endogenous GFP protein, turning infected cells green.

Purification was obtained by a three step chromatography of the media: cation exchange followed by metal-affinity and size exclusion chromatographies (Figure 2E). Several milligrams of protein were routinely obtained per liter of culture supernatant and the obtained protein was used for subsequent experiments.

Confirmation of disulfide bonds by mass-spectrometry

By analysing the recombinant human STC1-HT produced in the baculovirus system by ESI/Q-TOF analysis we were able to identify and assign the peptides that resulted from enzymatic digestion either with trypsin or chymotrypsin in the oxidized and/or reduced forms (Table 2, [see Additional file 1, 2 and 3]). In brief, the data show the existence of peptides having mass compatible with the presence of the previously predicted disulfide bonds for the salmon STC1. In Table 2, the first column gives the disulfide bridge in question and the last four columns give respectively the expected and experimentally determined peptide masses. In conclusion, all disulfide bridges except for one could be directly demonstrated. Still Cys_{45}-Cys_{59} could be evidenced indirectly, since the mass of the peptide shown in line one of Table 2 is compatible with this interpretation. Furthermore, after chemical digestion with formic acid, Cys_{202} could be unambiguously assigned as the Cys residue responsible for the dimerization of human STC1 (Table 2, [see Additional file 1, 2 and 3]).

Analysis of secondary structure

Such a relatively high content predicted by *in silico* analysis (Figure 1) is supposed to be readily detected by circular dichroism spectroscopy of the protein, so the content of secondary structure elements in recombinant human STC1-HT was determined by circular dichroism spectroscopy. Figure 3 shows the spectrum of purified STC1

Table 2: Identification of signature peptide sequences of STC1-HT for the assignment of the intra- and intermolecular disulfide bonds.

Disulfide Bond	Sequence of peptides	Protease	Mass			
			Theoretical	Observed (Expected)		
				[M+2H]	[M+3H]	[M+4H]
C_{45}-C_{59}; C_{54}-C_{74}; C_{65}-C_{114}	**C**$_{45}$LNSAL...ID**C**K$_{75}$ **C**$_{114}$STFQR$_{119}$	Trypsin	3981.51			996.22 (996.38)
C_{54}-C_{74}	Q$_{51}$VG**C**GAFA$_{57}$ D$_{72}$I**C**KSF$_{77}$	Chymotrypsin	1389.61	695.95 (695.81)	464.24 (464.21)	
C_{65}-C_{114}	E$_{61}$NST**C**...GMY$_{71}$ A$_{110}$IRR**C**STF$_{117}$	Chymotrypsin	2184.89		729.36 (729.30)	547.26 (547.23)
C_{98}-C_{128}	**C**$_{98}$IANGVTSK$_{106}$ M$_{120}$IAE...**C**YSK$_{131}$	Trypsin	2318.06		773.73 (773.69)	580.56 (580.52)
C_{98}-C_{128}	K$_{97}$**C**IA...SKVF$_{108}$ Q$_{118}$RMIA...EE**C**Y$_{129}$	Chymotrypsin	2761.32		921.17 (921.45)	691.14 (691.34)
C_{135}-C_{170}	L$_{132}$NV**C**SIAK$_{139}$ S$_{166}$LLE**C**...TIR$_{179}$	Trypsin	2424.19		809.12 (809.07)	607.08 (607.05)
Disulfide Bond	**Sequence of peptides**	**Chemical Reagent**	**Mass**			
			Theoretical	**Observed (Expected)**		
				[M+H]		
C_{202}-C_{202}*	D$_{200}$H**C**AQTHPRA$_{209}$ D$_{200}$H**C**AQTHPRA$_{209}$	Formic acid	2266.98	2268.11 (2267.99)		

Samples were digested by trypsin or chymotrypsin with or without dithiotreitol and iodoacetamide, separated by UPLC and analyzed by ESI-QTOF; or digested with formic acid and analyzed by MALDI-QTOF. The presented mass is the monoisotopic. Dimer disulphide bond is indicated by asterisk (*) [see Additional file 1, 2 and 3].

recorded at 4°C. Purified protein presents negative ellipticity in the near-UV, with minima at 208 (-17.2 × 10^3 deg cm^2 $dmol^{-1}$) and 222 nm (-12.8 × 10^3 deg cm^2 $dmol^{-1}$). Deconvolution of the CD spectrum lead to the following estimation of the content of secondary structural elements: ∼52% of α-helices, ∼19% of β-sheets strands, ∼11% of turns and ∼18% unordered (NRMSD = 0,009) using the CDSSTR algorithm on the Dichroweb web server [65]. Consensus predictions of secondary structures shown in Figure 1 give values of about 37% of helix, 2.5% of strands and 65.5% of other structures (37% of coils and 28.5% of non-determined). Secondary structural predictors like PSIPRED are based on neural networks trained on known folds, and thus tend routinely to underestimation of the true helical and strand content, due to the fact that the reference databases are not complete. A more critical issue is the fact that no other protein of the family of STCs has its structure resolved. In conclusion both the prediction and the experimentally determined data are in reasonable agreement, since they demonstrate a relatively high content of alpha-helices in human STC1.

STC1 is a compact, slightly ellipsoidal dimer in solution

Dynamic Light Scattering (DLS) data of the recombinant STC1 sample showed a single and narrow peak, which is an indicative of a monodisperse solution of dimers.

The corrected and normalized experimental SAXS data are shown in Figure 4A, together with the GNOM curve fitting. The Guinier region providing an Rg value of 27.4 ± 0.8 Å is shown in the inset. The p(r) function resulting from these calculations is shown in Figure 4B, with an inset showing the Kratky representation of the intensity curve. The Kratky plot indicates a slightly compact conformation for STC1 in solution. The maximum dimension (D_{max}) value obtained was 90 Å and the Rg value, calculated from the p(r) function, was 27.8 ± 0.4 Å, in close agreement with that calculated from the Guinier approxi-

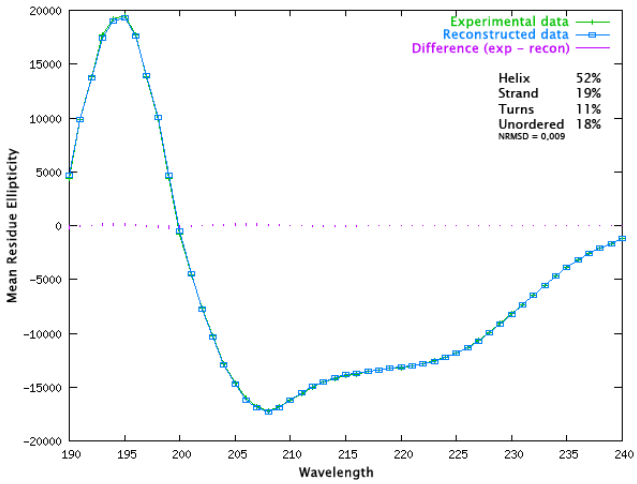

Figure 3
Circular Dichroism spectra of STC1-HT and deconvolution. Graph of the wavelength plotted against the mean residue elipticity of a sample at 5,5 mM in 10 mM MES; 33,3 mM NaCl pH 6,5 at 4°C. Data were deconvoluted with the CDSSTR program on the Dichroweb server. Note the two minima at 208 and 222 nm, which are typical of alpha-helix containing proteins. Reconstructed data are those derived from the Dichroweb database.

mation. As it can be noted from the p(r) function shape, STC1 has a slightly elongated shape.

Using BSA as a reference sample, the molecular mass for STC1 HT, estimated from the SAXS data, was ~54 kDa. This value is in agreement with the prediction of the protein being a dimer, since the theoretically calculated molecular mass of the monomer was ~27 kDa (calculated from the amino acids sequence using ProtParam tool [66]).

The dimerization was also confirmed both by mass spectrometry (see above) and by size exclusion chromatography (data not shown).

Low resolution ab initio *SAXS-based models for STC1*

The low resolution models for STC1 are presented in figure 5. Those models were derived from the experimental SAXS data imposing a 2 point symmetry constraint (P2). Additional models calculated without symmetry constraint (P1) presented very similar molecular envelopes. The calculated values of the Normalized Spatial Discrepancy (NSD), which is an indicator of the difference between models, gave values of ~0.6 for P1 vs. P2 DAMMIN models and ~0.8 for P1 vs. P2 GASBOR models, suggesting a low discrepancy. In view of this result, all model calculations were performed using a 2 point symmetry constraint. After several runs performed with the program DAMMIN, the averaged and filtered (with the corrected excluded volume) *dummy atom* model for STC1 is shown in Figure 5A. The NSD values for the set of 10 models ranged from 0.60 to 0.69, which are considered reasonable values [67]. This low resolution model shows the expected elongated shape for the protein dimer. The most typical and recurrent *dummy residue* model resulting from the calculation with the program GASBOR is shown in Figure 5B. The NSD values for this set of 10 calculations ranged from 0.82 to 0.87, which are also quite reasonable. This last approach produced an improved molecular envelope for STC1. Comparing the results, both molecular envelopes obtained for STC1 presented a similar shape and confirmed the elongated conformation for the dimer.

Conclusion

Our data provided the first low resolution 3D structure of human STC1 protein in solution. SAXS experiments indicated that STC1 forms a dimer of slightly elongated shape in solution. Circular dichroism spectroscopy confirmed the prediction of a high alpha-helical content and we could also confirm by mass spectrometry the highly conserved disulfide pattern, previously described in fish STC1[39]. Disulfide bonds are formed between the same 10 of the 11 conserved Cys, in the same fashion, leaving the C-terminal Cys 202 free to engage in dimer formation. None of our data explain the composition or structure of "bigSTC1" previously reported to appear in certain tissues [19,25,46-49]. Indeed, our results only show the formation of dimers (STC_{50}), by several independent methods. In human cells however, we may have additional contributions from possible post-translational modifications or alternative splice variants of the pre-mRNA encoding STC1, which may contribute to the appearance of the higher molecular weight forms. Further experiments are required to characterize big STC1 at the molecular level and point out its differences with the canonical dimeric human STC1.

Methods

In silico *sequence analysis*

We analyzed the human STC1 sequence as a query in six different secondary structure prediction databases (PredictProtein/PROF [51], PsiPRED [52], Predator [53], SOPMA [54], SSPro [55] and JCFO [56]). We also performed some predictions about ordered or disordered regions within the sequence using FoldIndex [57] and DisEMBL [58]) as well as GlobPlot [59], a predictor for globular regions. Additionally, some predictions about post-translational modifications were done and compared to previous published data. N-glycosylation sites were predicted by NetGlyc [62]. For phosphorylation we combined prediction data from NetPhos [63] and NetPhosK [64]. With PredictProtein/PHD Acc [51], we predicted whether residues are exposed to solvent or buried.

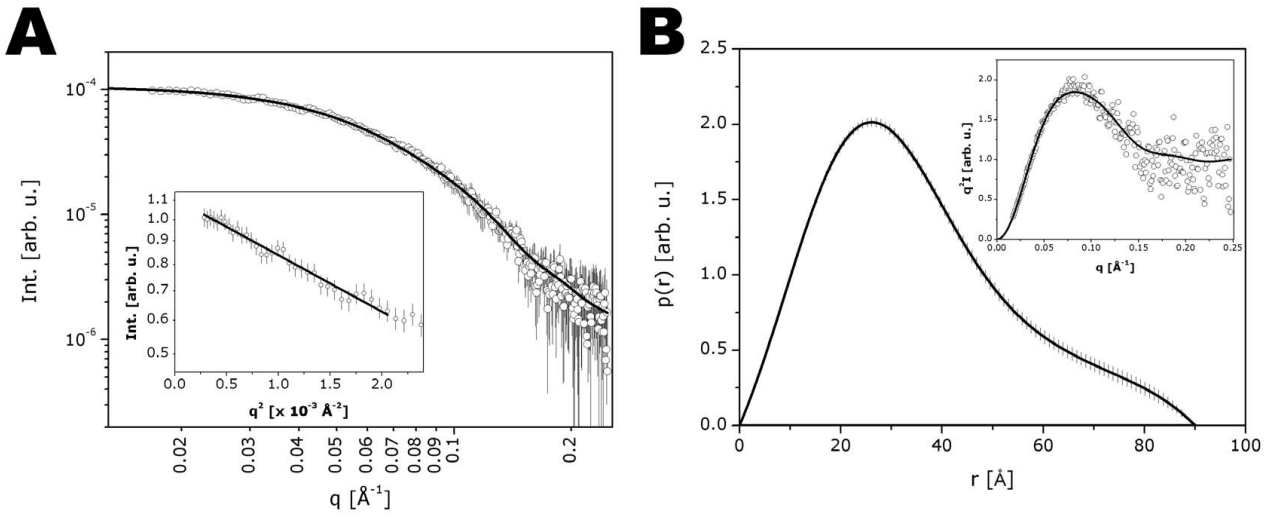

Figure 4
Experimental Small Angle X-ray Scattering (SAXS) curves for recombinant STC1-HT protein. (A) Experimental scattering curve of STC1-HT (open circles) and the theoretical fitting (solid line) by using the program GNOM. *Inset*: Guinier Region. (B) Pair-distance distribution function p(r). *Inset*: Kratky representation of the intensity curve.

Finally, in order to screen for lysine residues predicted which may be sumoylated in STC1 we used SUMOplot™ http://www.abgent.com/tools/sumoplot.

Cloning of STC1 cDNA

Full-length STC1 (Genbank NM_003155) gene was amplified from normal bone marrow stromal cells using primers STC1 F (5' aaggatccAGAATGCTCCAAAACTCAGC 3') and STC1 R (5' ccgaattCCTCTCCCTGGTTATGCAC 3') and cloned into vector pGEM resulting in plasmid **pGEM-STC1**. In order to obtain all constructs we used pGEM-STC1 as template and cloned PCR amplified products into pGEM plasmid: for **pGEM-STC1 ΔN_{term}**(STC1 lacking the first 22 amino acids) we used primers STC1 ΔN_{term} F (5' aaggatccCAGAATGACTCTGTGAGCCC 3') and STC1 R; for **pGEM-STC1 full without stop** (STC1 without stop-codon) we used primers STC1 F and STC1 no stop R (5' acaagcttCCTCTCCCTGGTaATGCAC 3'); for **pGEM-CSTC1** (C terminal of STC1 consisting of residues from 129 to 247) were used primers CSTC1 F (5' ggatccTACAG-CAAGCTGAATGTGTG 3') and CSTC1 R (5' gaattcTTAT-GCACTCTCATGGGATG 3'). Capital letters indicate sequence identical to STC1 cDNA, small caps letters indicate sequence non-identical to template. All pGEM constructs were verified by DNA sequencing in order to ascertain the correct nucleotide sequence. pGEM-STC1 ΔN_{term} and pGEM-CSTC1 were digested with BamHI and EcoRI and the resulting inserts were cloned into pET28a-His-Tev or pET28a-GST-Tev [68] previously digested with the same endonucleases. This resulted in pET-HT-STC1 ΔN_{term}, pET-HT-CSTC1, and the pET-GST-CSTC1 constructs. pGEM-STC1 full without stop was digested with BamHI and HindIII and cloned into a pFastBAC Dual+EGFP (pFBDg), which had the EGFP cDNA cloned under p10 promoter, digested with same endonucleases to insert STC1 under polyhedron promoter. Subsequently a pair of oligonucleotides (5'AGCTTGGAAAACCTGTATT TTCAGGGCCATCACCATCACCATCACCGG 3' and 5'AG CTCCGGTGATGGTGATGGTGATCGCCCTGAAAATA CA GGTTTTCCA 3') previously annealed was added to generate a linker consisting of a TEV protease site and a 6 × His-tag (HT) at the C-terminal, resulting in the pFBDg-STC1-HT construct. Other constructs mentioned in the text were generated by using the same methodology.

Expression and purification of STC1

Production of the recombinant 6 × His- or GST-STC1 fusion constructs in *E. coli* BL21 strain and subsequent purification trials were performed as described previously for other recombinant proteins [69,70].

High Five™ (Invitrogen) cells were adapted to grow in suspension culture in Express Five™ serum free media (Gibco) supplemented with 20 mM L-Glutamine (Gibco) and 1× PenStrep (Gibco). The stock cell culture was maintained and passaged in a 28°C incubator (ThermoForma). For STC1-HT production High Five cells were scaled up from the stock culture to a cell density of 1 × 10^6 in two 2L Erlenmeyer flasks containing 500 mL each and incubated at a shaker at 26°C at 140 rpm. Twelve hours post inoculation, the cells were infected with the recombinant baculo virus, at a multiplicity of infection (m.o.i.) between 3

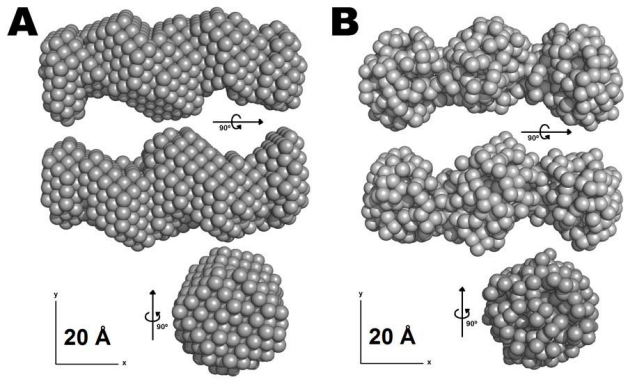

Figure 5
Low resolution *ab initio* model of STC1-HT derived from SAXS data. (A) Three selected views of the average and filtered *dummy atoms* model (DAMMIN). (B) Three selected views of the *dummy residues* model (GASBOR). The models were displayed by the PyMOL program [80].

and 4 plaque-forming unit (pfu) per cell. Baculovirus-infected High Five culture media were harvested after 48 hours post-infection by centrifugation at 500 × g for five minutes and cell-free supernatant containing secreted STC1-HT was used for purification. To the baculovirus supernatant a 1 M MES stock solution was added to bring the solution to a final concentration of 50 mM MES pH 6.5 (IEX buffer). The solution was filtered through a 0.45 μm MCE membrane (Fisherbrand) and loaded onto a water-jacketed chilled (4°C) XK26/20 (Pharmacia Biotech/GE) column previously packed with SP Sepharose FF (Pharmacia Biotech/GE) at a flow rate of 1 mL/min using a peristaltic pump (Biologic LP Biorad). Column was transferred to an ÄKTA FPLC system (GE) for protein elution using a 01 M gradient of NaCl in IEX buffer. Fractions eluted from a conductivity of 30 mS/cm onward, contained most of stanniocalcin 1 protein and were pooled. This pool was directly loaded onto a pre-packed HisTrap crude FF 5 mL (GE) column, equilibrated with 50 mM MES pH 6.5, 500 mM NaCl (affinity buffer). After injection of sample the column was washed with six column volume (CV) of affinity buffer, with three CV of affinity buffer containing 250 mM Imidazole and finally with four CV of affinity buffer containing 1 M Imidazole. This last pool of fractions containing most of stanniocalcin was concentrated using an Amicon Ultra-15 Centrifugal Filter Unit with Ultracel-10 membrane of 5,000 NMWL (Millipore) on a swing-rotor at 4°C and then 500 μL applied to a water-jacketed chilled (4°C) Superdex 200 pg 16/60 (GE) column, pre-equilibrated with 60 mM MES 600 mM NaCl pH 6.5 (SizeEx buffer) with a flow rate of 0.5 mL/min. Protein eluted at a single peak between 70 and 80 mL was analyzed by SDS-PAGE, pooled, concentrated and kept in SizeEx buffer at 4°C. The purity of the recombinant STC1 protein was confirmed by mass spectrometry analysis, which resulted in the exclusive identification of STC1 peptides (data not shown).

Disulfide bond and molecular mass analysis

Samples digested by trypsin or chymotrypsin, treated or not with dithiotreitol and iodoacetamide, were analyzed by using ultra-performance liquid chromatography (UPLC NanoAcquity, Waters) coupled with eletrospray ionization quadrupole time-of-flight tandem mass spectrometer (ESI-QTOF Ultima, Waters/Micromass). Samples chemically digested by formic acid [71], treated or not with dithiotreitol and iodoacetamide, were analyzed using MALDI-QTOF (Q-Tof Premier, Waters/Micromass). Data were analyzed by the MassLynx software package.

Circular Dischroism

Circular dichroism spectra were recorded at 4°C between 190 and 260 nm on a J-810 Jasco spectropolarimeter equipped with a Peltier-type system PFD 425S using a quartz cuvette of 10 mm path length, with a 50 nm/min scanning speed and a band-width of 0.5 nm. Twenty spectra of purified STC1-HT at 2.77 μM in dilution buffer (10 mM MES 33.3 mM NaCl pH6.5) were averaged and corrected from the baseline for buffer solvent contribution. Experimental data were analyzed using CDSSTR on Dychroweb web server [65].

Small Angle X-Ray Scattering and Analysis

Before the analysis, the sample was inspected by dynamic light scattering (DLS) to test the monodispersity of the solution. After that, the sample was centrifuged at 20.000 × g for 30 min at 4°C to remove any possible aggregates. The small-angle X-ray scattering experiments were performed at the D02A-SAXS2 beam line at LNLS. The measurements were performed at 4°C under temperature-controlled conditions (via water circulation) using a 1 mm path length cell with mica windows and a monochromatic X-ray beam (wavelength of λ = 1.488 Å). The X-ray patterns were recorded using a two-dimensional position-sensitive MARCCD detector and a sample-to-detector distance of 902 mm, resulting in a useful scattering vector range of $0.015 Å^{-1} < q < 0.25 Å^{-1}$, where q is the magnitude of the **q**-vector defined by $q = (4\pi/\lambda)\sin\theta$ (2θ is the scattering angle). Three successive frames of 300 seconds each and one frame of 30 minutes were recorded. The measurements were performed with two different concentrations for the sample in MES buffer (60 mM MES 200 mM NaCl pH 6.5): 0.15 and 0.18 mg/mL, both measured using the BCA™ Protein Assay Kit (Pierce). The buffer scattering curves were recorded keeping the same conditions used for the sample. The intensity curves were individually corrected for detector response and scaled by the incident beam intensity and sample absorption. Subsequently, buffer scattering was subtracted from the corresponding

sample scattering. The resulting curves were inspected for radiation-induced damage, but no such effect was observed. After scaling the curves for concentration, no concentration effect was observed. A 10 mg/ml BSA (66 kDa) solution in the same sample buffer was used as molecular mass standard sample to estimated the molecular mass of STC1-HT. This value was inferred from the ratio of the extrapolated values of the intensity at the origin, I(0), from both sample and BSA solutions scattering [72,73].

The first analysis was the evaluation of the radius of gyration (Rg) using the Guinier approximation: $I(q) = I(0)\exp\left(-q^2R_g^2/3\right)$ for $qR_g < 1$ [74-76]. The Rg was also calculated from the pair distance distribution function, p(r), which was obtained by indirect Fourier transform of the intensity curve using the program GNOM [77]. The p(r) function also provided the maximum dimension (D_{max}) of the molecule, Moreover, a Kratky representation [75,76] of the intensity curve ($q^2I(q)$ vs. q) was used to analyze the compactness of the protein conformation.

Ab initio *SAXS-based modeling*

The low resolution models for STC1 were restored from the SAXS intensity curves using two different approaches. In the first one, implemented by the program DAMMIN [78], the protein was represented as an assembly of densely packed spherical beads (*dummy atoms*). Using simulated annealing, the program starts from a random configuration of beads and searches for a configuration that best fits the experimental pattern. Ten calculations were performed and the normalized spatial discrepancies (NSD) [67] values among them were evaluated using the DAMAVER suite. When the NSD values are not so different, an averaged and filtered model structure (with the correct excluded volume) emerges from this calculation. The second approach, in which generally a better model is obtained, was implemented using the program GASBOR [79]. In this approach, the protein is represented as a chain of *dummy residues* (DRs). The number of DRs is usually known *a priori* from the protein amino acid sequence. Starting from a randomly distributed gas of DRs inside a spherical volume of diameter D_{max}, a simulated annealing routine was employed to find a chain-compatible spatial distribution of DRs which fit the experimental scattering pattern. Ten different calculations were also performed and the NSD values were evaluated. In this case, there is no advantage in obtaining an average model because the GASBOR program uses a predefined number of DRs, which makes the average routine little effective in achieving an improvement of the model resolution. So, we present the most typical model (with the lowest NSD value). In both approaches, the models calculated with 2 point-symmetry constraint were very similar to those calculated without these constraints. For this reason, the results presented here are from the calculation with 2 point-symmetry constraint. Both models were displayed by the PyMOL program [80].

Authors' contributions

DMT and JK conceived and designed the experiments, analyzed the data and wrote the manuscript. DMT performed the experiments. JCS performed SAXS experiments and interpreted them together with ICLT. MSN performed and interpreted the mass spectrometry experiments. JK supervised the project. All authors read and approved the final version of the manuscript.

Additional material

Additional file 1

Original UPLC-ESI-QTOF and MALDI-QTOF data (a). *Spectra of the trypsin data presented in Table 2 (part a)*
Click here for file
[http://www.biomedcentral.com/content/supplementary/1472-6807-9-57-S1.ppt]

Additional file 2

Original UPLC-ESI-QTOF and MALDI-QTOF data (b). *Spectra of the chymotrypsin data presented in Table 2 (part b)*
Click here for file
[http://www.biomedcentral.com/content/supplementary/1472-6807-9-57-S2.ppt]

Additional file 3

Original UPLC-ESI-QTOF and MALDI-QTOF data (c). *Spectra of the formic acid data presented in Table 2 (part c)*
Click here for file
[http://www.biomedcentral.com/content/supplementary/1472-6807-9-57-S3.ppt]

Acknowledgements

Financially supported by: Fundação de Amparo à Pesquisa do Estado São Paulo, the Conselho Nacional de Pesquisa e Desenvolvimento and the LNLS. We thank Maria Eugenia R. Camargo for technical assistance, Adriana Cristina Alves Pinto for help with chromatography, Rodrigo Martinez for the technical support at the SAXS2 beamline, Renata Rocha de Oliveira for support with CD data acquisition and Dr. Nilson Zanchin for access to mass spectrometer lab.

References

1. Wagner GF, DiMattia GE: **The stanniocalcin family of proteins.** *J Exp Zoolog A Comp Exp Biol* 2006, **305:**769-780.
2. Wendelaar Bonga SE, Smits PW, Flik G, Kaneko T, Pang PK: **Immunocytochemical localization of hypocalcin in the endocrine cells of the corpuscles of Stannius in three teleost species (trout, flounder and goldfish).** *Cell Tissue Res* 1989, **255:**651-656.
3. Pandey AC: **Evidence for general hypocalcemic hormone from the stannius corpuscles of the freshwater catfish Ompok bimaculatus (Bl).** *Gen Comp Endocrinol* 1994, **94:**182-185.

4. Wagner GF, Guiraudon CC, Milliken C, Copp DH: **Immunological and biological evidence for a stanniocalcin-like hormone in human kidney.** *Proc Natl Acad Sci USA* 1995, **92:**1871-1875.
5. Tanega C, Radman DP, Flowers B, Sterba T, Wagner GF: **Evidence for stanniocalcin and a related receptor in annelids.** *Peptides* 2004, **25:**1671-1679.
6. Hang X, Balment RJ: **Stanniocalcin in the euryhaline flounder (Platichthys flesus): primary structure, tissue distribution, and response to altered salinity.** *Gen Comp Endocrinol* 2005, **144:**188-195.
7. Shin J, Oh D, Sohn YC: **Molecular characterization and expression analysis of stanniocalcin-1 in turbot (Scophthalmus maximus).** *Gen Comp Endocrinol* 2006, **147:**214-221.
8. Madsen KL, Tavernini MM, Yachimec C, Mendrick DL, Alfonso PJ, Buergin M, Olsen HS, Antonaccio MJ, Thomson AB, Fedorak RN: **Stanniocalcin: a novel protein regulating calcium and phosphate transport across mammalian intestine.** *Am J Physiol* 1998, **274:**G96-102.
9. Olsen HS, Cepeda MA, Zhang QQ, Rosen CA, Vozzolo BL: **Human stanniocalcin: a possible hormonal regulator of mineral metabolism.** *Proc Natl Acad Sci USA* 1996, **93:**1792-1796.
10. Wagner GF, Vozzolo BL, Jaworski E, Haddad M, Kline RL, Olsen HS, Rosen CA, Davidson MB, Renfro JL: **Human stanniocalcin inhibits renal phosphate excretion in the rat.** *J Bone Miner Res* 1997, **12:**165-171.
11. Gagliardi AD, Kuo EY, Raulic S, Wagner GF, DiMattia GE: **Human stanniocalcin-2 exhibits potent growth-suppressive properties in transgenic mice independently of growth hormone and IGFs.** *Am J Physiol Endocrinol Metab* 2005, **288:**E92-105.
12. Moore EE, Kuestner RE, Conklin DC, Whitmore TE, Downey W, Buddle MM, Adams RL, Bell LA, Thompson DL, Wolf A, *et al.*: **Stanniocalcin 2: characterization of the protein and its localization to human pancreatic alpha cells.** *Horm Metab Res* 1999, **31:**406-414.
13. Ito D, Walker JR, Thompson CS, Moroz I, Lin W, Veselits ML, Hakim AM, Fienberg AA, Thinakaran G: **Characterization of stanniocalcin 2, a novel target of the mammalian unfolded protein response with cytoprotective properties.** *Mol Cell Biol* 2004, **24:**9456-9469.
14. Ishibashi K, Miyamoto K, Taketani Y, Morita K, Takeda E, Sasaki S, Imai M: **Molecular cloning of a second human stanniocalcin homologue (STC2).** *Biochem Biophys Res Commun* 1998, **250:**252-258.
15. Chang AC, Reddel RR: **Identification of a second stanniocalcin cDNA in mouse and human: stanniocalcin 2.** *Mol Cell Endocrinol* 1998, **141:**95-99.
16. Varghese R, Wong CK, Deol H, Wagner GF, DiMattia GE: **Comparative analysis of mammalian stanniocalcin genes.** *Endocrinology* 1998, **139:**4714-4725.
17. Chang AC, Jellinek DA, Reddel RR: **Mammalian stanniocalcins and cancer.** *Endocr Relat Cancer* 2003, **10:**359-373.
18. McCudden CR, James KA, Hasilo C, Wagner GF: **Characterization of mammalian stanniocalcin receptors. Mitochondrial targeting of ligand and receptor for regulation of cellular metabolism.** *J Biol Chem* 2002, **277:**45249-45258.
19. Paciga M, McCudden CR, Londos C, DiMattia GE, Wagner GF: **Targeting of big stanniocalcin and its receptor to lipid storage droplets of ovarian steroidogenic cells.** *J Biol Chem* 2003, **278:**49549-49554.
20. Lafeber FP, Flik G, Wendelaar Bonga SE, Perry SF: **Hypocalcin from Stannius corpuscles inhibits gill calcium uptake in trout.** *Am J Physiol* 1988, **254:**R891-R896.
21. Hanssen RG, Lafeber FP, Flik G, Wendelaar Bonga SE: **Ionic and total calcium levels in the blood of the European eel (Anguilla anguilla): effects of stanniectomy and hypocalcin replacement therapy.** *J Exp Biol* 1989, **141:**177-186.
22. Wendelaar Bonga SE, Pang PK: **Control of calcium regulating hormones in the vertebrates: parathyroid hormone, calcitonin, prolactin, and stanniocalcin.** *Int Rev Cytol* 1991, **128:**139-213.
23. Chang AC, Janosi J, Hulsbeek M, de Jong D, Jeffrey KJ, Noble JR, Reddel RR: **A novel human cDNA highly homologous to the fish hormone stanniocalcin.** *Mol Cell Endocrinol* 1995, **112:**241-247.
24. Worthington RA, Brown L, Jellinek D, Chang AC, Reddel RR, Hambly BD, Barden JA: **Expression and localisation of stanniocalcin 1 in rat bladder, kidney and ovary.** *Electrophoresis* 1999, **20:**2071-2076.
25. Paciga M, Watson AJ, DiMattia GE, Wagner GF: **Ovarian stanniocalcin is structurally unique in mammals and its production and release are regulated through the luteinizing hormone receptor.** *Endocrinology* 2002, **143:**3925-3934.
26. Serlachius M, Alitalo R, Olsen HS, Andersson LC: **Expression of stanniocalcin-1 in megakaryocytes and platelets.** *Br J Haematol* 2002, **119:**359-363.
27. Yoshiko Y, Aubin JE: **Stanniocalcin 1 as a pleiotropic factor in mammals.** *Peptides* 2004, **25:**1663-1669.
28. Tohmiya Y, Koide Y, Fujimaki S, Harigae H, Funato T, Kaku M, Ishii T, Munakata Y, Kameoka J, Sasaki T: **Stanniocalcin-1 as a novel marker to detect minimal residual disease of human leukemia.** *Tohoku J Exp Med* 2004, **204:**125-133.
29. Wascher RA, Huynh KT, Giuliano AE, Hansen NM, Singer FR, Elashoff D, Hoon DS: **Stanniocalcin-1: a novel molecular blood and bone marrow marker for human breast cancer.** *Clin Cancer Res* 2003, **9:**1427-1435.
30. Serlachius M, Zhang KZ, Andersson LC: **Stanniocalcin in terminally differentiated mammalian cells.** *Peptides* 2004, **25:**1657-1662.
31. Serlachius M, Andersson LC: **Upregulated expression of stanniocalcin-1 during adipogenesis.** *Exp Cell Res* 2004, **296:**256-264.
32. Yoshiko Y, Maeda N, Aubin JE: **Stanniocalcin 1 stimulates osteoblast differentiation in rat calvaria cell cultures.** *Endocrinology* 2003, **144:**4134-4143.
33. Franzen AM, Zhang KZ, Westberg JA, Zhang WM, Arola J, Olsen HS, Andersson LC: **Expression of stanniocalcin in the epithelium of human choroid plexus.** *Brain Res* 2000, **887:**440-443.
34. Jiang WQ, Chang AC, Satoh M, Furuichi Y, Tam PP, Reddel RR: **The distribution of stanniocalcin 1 protein in fetal mouse tissues suggests a role in bone and muscle development.** *J Endocrinol* 2000, **165:**457-466.
35. Zhang KZ, Westberg JA, Paetau A, von Boguslawsky K, Lindsberg P, Erlander M, Guo H, Su J, Olsen HS, Andersson LC: **High expression of stanniocalcin in differentiated brain neurons.** *Am J Pathol* 1998, **153:**439-445.
36. Filvaroff EH, Guillet S, Zlot C, Bao M, Ingle G, Steinmetz H, Hoeffel J, Bunting S, Ross J, Carano RA, *et al.*: **Stanniocalcin 1 alters muscle and bone structure and function in transgenic mice.** *Endocrinology* 2002, **143:**3681-3690.
37. Varghese R, Gagliardi AD, Bialek PE, Yee SP, Wagner GF, DiMattia GE: **Overexpression of human stanniocalcin affects growth and reproduction in transgenic mice.** *Endocrinology* 2002, **143:**868-876.
38. Chang AC, Dunham MA, Jeffrey KJ, Reddel RR: **Molecular cloning and characterization of mouse stanniocalcin cDNA.** *Mol Cell Endocrinol* 1996, **124:**185-187.
39. Hulova I, Kawauchi H: **Assignment of disulfide linkages in chum salmon stanniocalcin.** *Biochem Biophys Res Commun* 1999, **257:**295-299.
40. Ishibashi K, Imai M: **Prospect of a stanniocalcin endocrine/paracrine system in mammals.** *Am J Physiol Renal Physiol* 2002, **282:**F367-F375.
41. Gerritsen ME, Wagner GF: **Stanniocalcin: no longer just a fish tale.** *Vitam Horm* 2005, **70:**105-135.
42. Amemiya Y, Marra LE, Reyhani N, Youson JH: **Stanniocalcin from an ancient teleost: a monomeric form of the hormone and a possible extracorpuscular distribution.** *Mol Cell Endocrinol* 2002, **188:**141-150.
43. Amemiya Y, Irwin DM, Youson JH: **Cloning of stanniocalcin (STC) cDNAs of divergent teleost species: Monomeric STC supports monophyly of the ancient teleosts, the osteoglossomorphs.** *Gen Comp Endocrinol* 2006, **149:**100-107.
44. Wagner GF, DiMattia GE, Davie JR, Copp DH, Friesen HG: **Molecular cloning and cDNA sequence analysis of coho salmon stanniocalcin.** *Mol Cell Endocrinol* 1992, **90:**7-15.
45. Yamashita K, Koide Y, Itoh H, Kawada N, Kawauchi H: **The complete amino acid sequence of chum salmon stanniocalcin, a calcium-regulating hormone in teleosts.** *Mol Cell Endocrinol* 1995, **112:**159-167.
46. Hasilo CP, McCudden CR, Gillespie JR, James KA, Hirvi ER, Zaidi D, Wagner GF: **Nuclear targeting of stanniocalcin to mammary gland alveolar cells during pregnancy and lactation.** *Am J Physiol Endocrinol Metab* 2005, **289:**E634-E642.

47. Paciga M, James K, Gillespie JR, Wagner GF: **Evidence for cross-talk between stanniocalcins.** *Can J Physiol Pharmacol* 2005, **83:**953-956.
48. Paciga M, Hirvi ER, James K, Wagner GF: **Characterization of big stanniocalcin variants in mammalian adipocytes and adrenocortical cells.** *Am J Physiol Endocrinol Metab* 2005, **289:**E197-E205.
49. Paciga M, DiMattia GE, Wagner GF: **Regulation of luteal cell big stanniocalcin production and secretion.** *Endocrinology* 2004, **145:**4204-4212.
50. Jellinek DA, Chang AC, Larsen MR, Wang X, Robinson PJ, Reddel RR: **Stanniocalcin 1 and 2 are secreted as phosphoproteins from human fibrosarcoma cells.** *Biochem J* 2000, **350(Pt 2):**453-461.
51. Rost B, Yachdav G, Liu J: **The PredictProtein server.** *Nucleic Acids Res* 2004, **32:**W321-W326.
52. Bryson K, McGuffin LJ, Marsden RL, Ward JJ, Sodhi JS, Jones DT: **Protein structure prediction servers at University College London.** *Nucleic Acids Res* 2005, **33:**W36-W38.
53. Frishman D, Argos P: **Seventy-five percent accuracy in protein secondary structure prediction.** *Proteins* 1997, **27:**329-335.
54. Geourjon C, Deleage G: **SOPMA: significant improvements in protein secondary structure prediction by consensus prediction from multiple alignments.** *Comput Appl Biosci* 1995, **11:**681-684.
55. Cheng J, Randall AZ, Sweredoski MJ, Baldi P: **SCRATCH: a protein structure and structural feature prediction server.** *Nucleic Acids Res* 2005, **33:**W72-W76.
56. Meiler J, Baker D: **Coupled prediction of protein secondary and tertiary structure.** *Proc Natl Acad Sci USA* 2003, **100:**12105-12110.
57. Prilusky J, Felder CE, Zeev-Ben-Mordehai T, Rydberg EH, Man O, Beckmann JS, Silman I, Sussman JL: **FoldIndex: a simple tool to predict whether a given protein sequence is intrinsically unfolded.** *Bioinformatics* 2005, **21:**3435-3438.
58. Linding R, Jensen LJ, Diella F, Bork P, Gibson TJ, Russell RB: **Protein disorder prediction: implications for structural proteomics.** *Structure* 2003, **11:**1453-1459.
59. Linding R, Russell RB, Neduva V, Gibson TJ: **GlobPlot: Exploring protein sequences for globularity and disorder.** *Nucleic Acids Res* 2003, **31:**3701-3708.
60. Ellard JP, McCudden CR, Tanega C, James KA, Ratkovic S, Staples JF, Wagner GF: **The respiratory effects of stanniocalcin-1 (STC-1) on intact mitochondria and cells: STC-1 uncouples oxidative phosphorylation and its actions are modulated by nucleotide triphosphates.** *Mol Cell Endocrinol* 2007, **264:**90-101.
61. Zhang J, Alfonso P, Thotakura NR, Su J, Buergin M, Parmelee D, Collins AW, Oelkuct M, Gaffney S, Gentz S, *et al.*: **Expression, purification, and bioassay of human stanniocalcin from baculovirus-infected insect cells and recombinant CHO cells.** *Protein Expr Purif* 1998, **12:**390-398.
62. Gupta R, Jung E, Brunak S: **Prediction of N-glycosylation sites in human proteins.** 2004 [http://www.cbs.dtu.dk/services/NetNGlyc/].
63. Blom N, Gammeltoft S, Brunak S: **Sequence and structure-based prediction of eukaryotic protein phosphorylation sites.** *J Mol Biol* 1999, **294:**1351-1362.
64. Blom N, Sicheritz-Ponten T, Gupta R, Gammeltoft S, Brunak S: **Prediction of post-translational glycosylation and phosphorylation of proteins from the amino acid sequence.** *Proteomics* 2004, **4:**1633-1649.
65. Whitmore L, Wallace BA: **DICHROWEB, an online server for protein secondary structure analyses from circular dichroism spectroscopic data.** *Nucleic Acids Res* 2004, **32:**W668-W673.
66. Gasteiger E, Gattiker A, Hoogland C, Ivanyi I, Appel RD, Bairoch A: **ExPASy: The proteomics server for in-depth protein knowledge and analysis.** *Nucleic Acids Res* 2003, **31:**3784-3788.
67. Volkov VV, Svergun DI: **Uniqueness of ab initio shape determination in small-angle scattering.** *J Appl Cryst* 2003, **36:**860-864.
68. Carneiro FR, Silva TC, Alves AC, Haline-Vaz T, Gozzo FC, Zanchin NI: **Spectroscopic characterization of the tumor antigen NY-REN-21 and identification of heterodimer formation with SCAND1.** *Biochem Biophys Res Commun* 2006, **343:**260-268.
69. Assmann EM, Alborghetti MR, Camargo ME, Kobarg J: **FEZ1 dimerization and interaction with transcription regulatory proteins involves its coiled-coil region.** *J Biol Chem* 2006, **281:**9869-9881.
70. Lanza DC, Trindade DM, Assmann EM, Kobarg J: **Over-expression of GFP-FEZ1 causes generation of multi-lobulated nuclei mediated by microtubules in HEK293 cells.** *Exp Cell Res* 2008, **314:**2028-2039.
71. Li A, Sowder RC, Henderson LE, Moore SP, Garfinkel DJ, Fisher RJ: **Chemical cleavage at aspartyl residues for protein identification.** *Anal Chem* 2001, **73:**5395-5402.
72. Orthaber D, ergmann A, Glatter O: **SAXS experiments on absolute scale with Kratky systems using water as a secondary standard.** *J Appl Cryst* 2000, **33:**218-255.
73. Mylonas E, Svergun DI: **Accuracy of molecular mass determination of proteins in solution by small-angle X-ray scattering.** *J Appl Cryst* 2007, **40:**s245-s249.
74. Guinier A, Fournet G: *Small angle scattering of X-rays* New York: John Wiley and Sons, Inc; 1955.
75. Glatter O, Kratky O: *Small Angle X-Ray Scattering* New York: Academic Press; 1982.
76. Feigin LA, Svergun DI: *Structure analysis by small-angle X-ray and neutron scattering* New York: Plenum Press; 1987.
77. Svergun DI: **Determination of the regularization parameter in indirect-transform methods using perceptual criteria.** *J Appl Cryst* 1992, **25:**495-503.
78. Svergun DI: **Restoring low resolution structure of biological macromolecules from solution scattering using simulated annealing.** *Biophys J* 1999, **76:**2879-2886.
79. Svergun DI, Petoukhov MV, Koch MH: **Determination of domain structure of proteins from X-ray solution scattering.** *Biophys J* 2001, **80:**2946-2953.
80. DeLano WL: **The PyMOL Molecular Graphics System.** 2002 [http://www.pymol.org].